Small-Signal Stability Assessment and Interaction Analysis for Bipolar DC Microgrids

Minrui Leng, *Student Member, IEEE*, Guohua Zhou, *Senior Member, IEEE*, Guodong Xu, Subham Sahoo, *Member, IEEE*, Xueshan Liu, *Member, IEEE*, Qun Zhou, Yue Yin, *Member, IEEE*, and Frede Blaabjerg, *Fellow, IEEE*

***Abstract*—Bipolarity in dc microgrids is desirable as it enhances the system's reliability and efficiency. However, the stability assessment for a bipolar dc microgrid is challenging due to the integration of a three-wire dc distribution line and numerous connected power converters, which is different from the stability analysis of a conventional unipolar dc microgrid. In this article, the basic form is arranged by a generalized voltage source or current source, and the simplified form is derived by looking into the different bus ports of a bipolar system in detail. Then, an impedance sum criteria-based stability conditions of different bus ports in the bipolar dc microgrid are proposed. To explore the mutual influence of the stability among different bus ports and investigate the stability issues caused by unbalanced loads connected to the symmetrical bus port, three cases are studied: 1) $\pm V_{\rm dc}$ bus ports are connected with balanced and unbalanced loads; 2) $-V_{\rm dc}$ bus port introduces the photovoltaic unit and the energy storage unit; and 3) the $2V_{\rm dc}$ bus port introduces the photovoltaic unit and the energy storage unit. Finally, a $\pm$24 V bipolar dc microgrid platform is set up to conduct experiments, verifying the accuracy and effectiveness of the stability evaluation method.**

***Index Terms*—Balanced and unbalanced loads, bipolar dc microgrid, mutual influence, stability assessment.**

I. Introduction

RENEWABLE energy sources are regarded as an efficient way to alleviate the environmental pollution caused by fossil fuels [1], [2]. Solar photovoltaics (PV), wind, and fuel cells (FCs) are popular clean energy resources that can be efficiently interfaced with distributed generation networks such as microgrids. Owing to higher efficiency, being able to provide a natural interface to renewable energy sources and hybrid energy storage, better compliance with consumer electronics, and disregarding issues related to synchronization, skin effect, and reactive power, dc microgrid is deemed as a huge potential asset for plenty of users [3], [4], [5], such as data centers, vehicular electric power systems, and dc-powered homes.

Driven by practical requirements of specific applications, there are two mainstream configurations for dc microgrids, namely the unipolar structure [6], [7] and the bipolar structure [8], [9]. Compared to the conventional unipolar dc microgrid, the bipolar dc microgrid generates two dc voltages using a three-wire structure, providing an option for loads to choose three different supply voltages through different connections to wires. If one wire snaps out, it is possible that the power is supplied by the other two lines and an auxiliary converter [9]. A typical bipolar dc microgrid is shown in Fig. 1. The bipolar configuration enables to transfer of more power per unit conductor cross-section with less conduction losses as compared to the unipolar configuration. Therefore, the bipolar dc microgrid system provides higher flexibility, reliability, and efficiency, which has been widely used in residential complexes and data center, such as the data center in the Intel Corporation and the intelligent industrial park [10], [11].

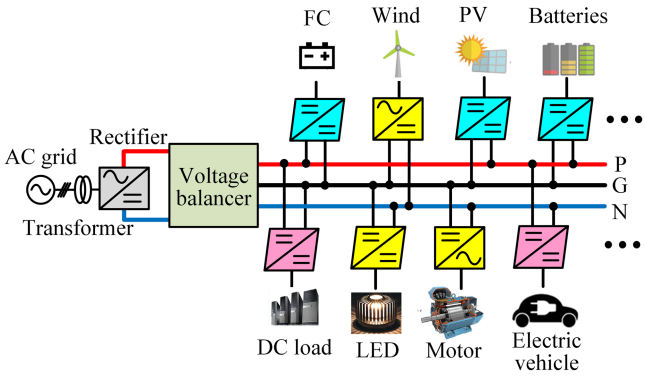

Fig. 1. Generic structure of a bipolar DC microgrid.

Manuscript received 7 August 2022; revised 30 October 2022; accepted 15 December 2022. Date of publication 6 January 2023; date of current version 14 February 2023. This work was supported in part by the National Natural Science Foundation of China under Grant 62271417, in part by the Youth Fund of Sichuan Province under Grant 23NSFSC3809, and in part by the Science and Technology Department of Sichuan Province under Grant 2022YFH0018. Recommended for publication by Associate Editor S. A. Khajehoddin. *(Corresponding author: Qun Zhou.)*

Minrui Leng, Xueshan Liu, Qun Zhou, and Yue Yin are with the College of Electrical Engineering, Sichuan University, Chengdu 610065, China (e-mail: mrleng_pece@163.com; xueshan5851@163.com; zhouqunsc@163.com; yyin2016@126.com).

Guohua Zhou is with the School of Electrical Engineering, Southwest Jiaotong University, Chengdu 611756, China (e-mail: eeghzhou@swjtu.edu.cn).

Guodong Xu is with the Texas Instruments Incorporated, Dallas 75266, TX USA (e-mail: xgd_pece@163.com).

Subham Sahoo and Frede Blaabjerg are with the Department of Energy Technology, Aalborg University, 9220 Aalborg, Denmark (e-mail: sssa@et.aau.dk; fbl@et.aau.dk).

Color versions of one or more figures in this article are available at https://doi.org/10.1109/TPEL.2022.3233397.

Digital Object Identifier 10.1109/TPEL.2022.3233397

TABLE I
COMPARISONS OF STABILITY ANALYSIS METHODS

Methods	Nyquist stability criterion [23]	Impedance specification methods [19, 24]	Impedance sum criteria [21]	Impedance-based local stability criterion [20]	Impedance-based stability assessment methodology [7]
Configurations	Cascaded system with single bus	Cascaded system with single bus	DC distributed power system with single bus	DC distributed power system with single bus	DC distributed power system with multiple buses
Theoretical bases and analysis tools	The minor loop gain, Nyquist diagrams and bode plots	The minor loop gain, bode plots	Cauchy's argument principle, pole-zero maps	The minor loop gain, bode plots	The minor loop gain, Nyquist diagrams
Advantages	Stability assessment for the "black-box" systems whose internal parameters are unknown	Intuitive and effective for stability investigation	Intuitive and effective for stability investigation and avoiding introducing open loop RHP poles in analysis	Providing a simple and general stability assessment	Providing an effective way to analyze the stability of dc distributed power system with two buses
Constraints	Not available for individual impedance shaping	Assuming fixed power flow direction	Assuming fixed power flow direction	complex to be extended	Being high dimensionality, unsuitable for plug-and-play applications

Increasing attention has been paid to bipolar dc microgrids due to the tremendous potential of their use in the development of dc distributed systems. The successive emergence of research [12], [13], [14], [15] for bipolar dc microgrids mainly include the grounding, protections against short circuit faults, and circuit topologies, aiming at how to construct a stable and reliable structure for bipolar dc microgrid. Microgrids, which are consisted of multiple converters, can become unstable due to the interactions of the converters [16], [17]. Adding a third wire to the conventional dc microgrids complicates the system interactions and can lead to new stability criteria. Tavakoli et al. [18] first proposed a multi-input multi-output analysis, which accurately captures the small-signal dynamics of bipolar dc microgrids and the mutual interactions between two bipolar terminals. However, this analysis incurs high dimensionality with the increasing number of power electronic converters and it is not suitable for plug-and-play applications. As a result, the stability investigation for bipolar dc microgrids is in starting stage, which needs to use the thinking way of conventional stability analysis methods as references.

The conventional stability analysis methods are extensively studied in recent years. The impedance-based analysis method was date back to 1976 and applied to design the input filter of a dc system [19]. The stability of the cascaded system can be evaluated at the precondition that the source converter and the load converter are defined. The literature about the extension of the impedance-based analysis method focus on two perspectives: 1) proposing improved impedance-based criteria; and 2) extending the impedance-based analysis to different systems which cannot be treated simply as the source converter and the load converter. Table I provides a comparison of the existing impedance-based stability analysis methods. On the one hand, a series of improved impedance specifications based on the forbidden region are reported to reduce the conservatism of the Middlebrook criterion. On the other hand, the impedance-based analysis method was extended to different systems, such as dc distributed power systems [20], hybrid energy storage systems [21], triple-stage cascaded dc systems [22], and multibus dc microgrids [7]. As it can be seen from Table I, impedance sum criteria are attractive due to being intuitive and effective for stability investigation and avoiding evaluating open loop RHP poles in system analysis, providing a theoretical reference for the analysis of bipolar dc microgrid.

In conclusion, though many efforts are devoted to impedance-based stability analysis, most of the works are directing at unipolar systems which cannot be directly applied to bipolar dc microgrids. Due to complex power flow modes and circuit configurations caused by the three-wire topology and the voltage balancer in bipolar dc microgrid, the stability assessment for the bipolar dc microgrid is a great challenge, which is not well-addressed so far.

Hence, this article proposes a simplified representation of the stability assessment method for bipolar dc microgrid based on the relationship of the three bus ports. By doing so, the stability of each bus port in a bipolar dc microgrid can be investigated separately. Three cases, namely 1) $\pm V_{\rm dc}$ bus ports connected with balanced and unbalanced load units; 2) $-V_{\rm dc}$ bus port connected with the PV unit and the energy storage unit; and 3) the $2V_{\rm dc}$ bus port connected with the PV unit and the energy storage unit, are conducted to establish the effectiveness of the proposed method. The stability interactions among these three bus ports are revealed. Moreover, some guidelines for stability, including the connection of load units, PV units, and energy storage units, are given.

The rest of this article is organized as follows. Section II describes the bipolar dc microgrid. In Section III, the stability assessment method of the bipolar dc microgrid is proposed. Section IV gives three case studies including the

experimental results to verify the effectiveness of the proposed method. Finally, Section V concludes this article.

II. Description of the Bipolar DC Microgrid

For a bipolar dc microgrid, there are three buses, i.e., P, N, and G, and the bus G is grounded, as shown in Fig. 1. The bipolar architecture for a dc microgrid offers interesting features over the conventional unipolar counterpart. It is seen that the utility ac voltage is converted to dc with the use of a distribution transformer and an active rectifier, also called a distribution converter. Then, at the dc level, the voltage balancer is connected and the system adopts a three-wire structure composed of the positive conductor (P), the negative conductor (N), and the neutral conductor (G). The voltage between the positive and negative poles is analogous to the line-to-line voltage, whereas the voltage of a pole with respect to the neutral connector is analogous to the phase-to-neutral one. This allows accommodating a wide set of distributed generators and loads with different voltage and power rating combinations in a single dc network. The role of the distribution converter is to provide an adjustable power factor, bidirectional power handling, high-quality input current and dc voltage, and reduced filtering requirements while simultaneously providing high reliability and a reduced device count. The main function of the voltage balancer is to balance the currents at the dc side, allowing the distribution converter to keep the voltages of the poles balanced to $V/2$. By relocating the energy consumption or generation, voltage balancing can be achieved for any operating condition. The most commonly used buck-boost type voltage balancer [12], [25], which regulates the inductor current to redistribute the unequal currents between poles and maintain the voltage balance.

As compared to the conventional unipolar dc microgrid, the bipolar dc microgrid can offer operation at multiple voltage levels ($\pm V_{\rm dc}$, $2V_{\rm dc}$), giving a flexible choice for the electrical equipment to connect to a relatively high voltage ($2V_{\rm dc}$) or lower voltage ($V_{\rm dc}$), as per their desired specifications. Owing to three-wire topology, the bipolar dc microgrids are characterized by flexible connections of loads and power units, as shown in Fig. 2. As it can be seen, except for connection type in Fig. 2(a)–(c), which shares similar connection way in unipolar dc microgrid, there are other six connection types, significantly increasing the complexity. Moreover, with the voltage balancer, the interactions between different bus ports are introduced. In addition, PV array, batteries, and loads units connected to different buses in various applications will arise complex power flow directions, making the existing impedance-based method invalid. Thus, we need to redefine the "source converter" and "load converter" according to complex power flow in a bipolar dc microgrid.

As a result, taking into different power flow directions and connections, exploring a general structure to describe the bipolar dc microgrid is important.

In relation to Fig. 3, Fig. 4 shows the detailed connection in a bipolar dc microgrid, which indicates the relationship between groups 1, 2, and 3. It can be seen that group 3 is directly supplied by the input voltage while groups 1 and 2 are supplied and interfaced through a voltage balancer. Even though we take the idea of a unipolar dc microgrid to classify bipolar dc microgrid as three groups because of the existence of a voltage balancer and three-wire topology, the stability analysis for bipolar dc microgrid is different from the conventional unipolar dc microgrid.

This article takes the bipolar dc microgrid with PV generation and energy storage as an example to illustrate that bipolar dc microgrid has various operations due to different control objectives, i.e., controlling output voltage and controlling the output power. If the PV array and batteries are included, the

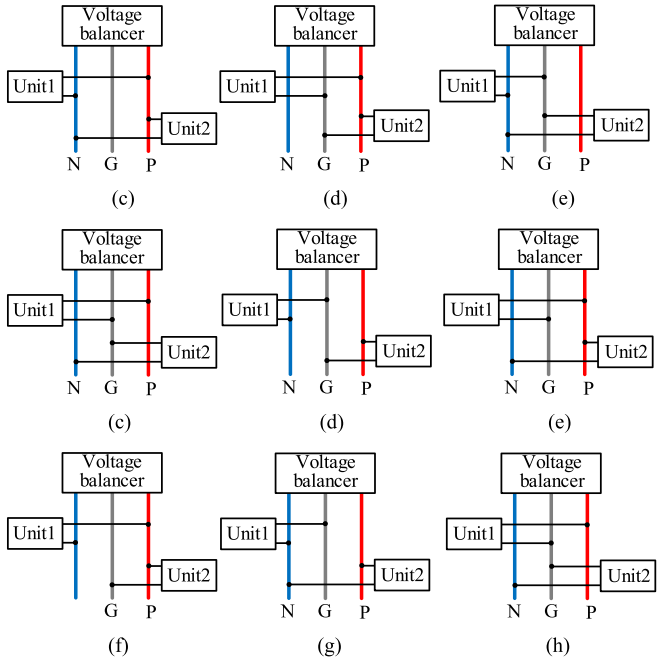

Fig. 2. Different connections of loads and power units in bipolar DC microgrid.

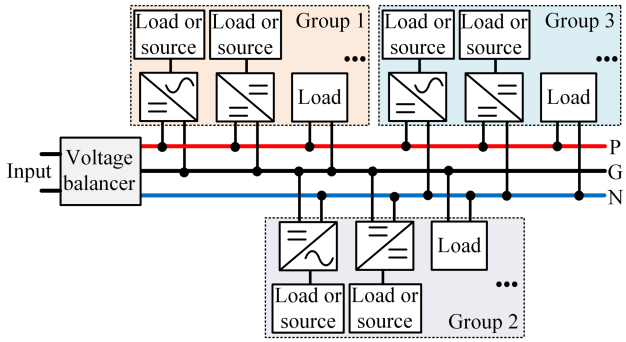

Fig. 3. Bipolar DC microgrid with three groups.

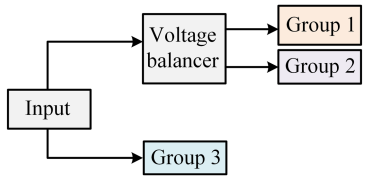

Fig. 4. Detailed connection of the bipolar DC microgrid.

TABLE II
DIFFERENT MODES FOR BIPOLAR DC MICROGRID

Units / Modes	Voltage balancer	PV unit	Battery unit
	Possible operations		
Mode I ~ Mode III ($P_l > P_o$)	provides energy to the load, adjusts $P_l + P_{pv} = P_o$	provides energy to battery or load by the maximum power point tracking (MPPT), by voltage limiting mode, adjusts $P_l + P_{pv} = P_o$	charged by the P_l - P_o power and PV unit power, fully charged, in floating charging
Mode IV ($P_l < P_o$, $P_l + P_{pv} < P_o$)	adjusts P_l and provides energy to the load	provides energy to the load by MPPT	discharged and provides energy to the load
Mode IV ~ Mode VII ($P_l < P_o$, $P_l + P_{pv} > P_o$)	provides energy to the load, adjusts $P_l + P_{pv} = P_o$	provides energy to battery or load by MPPT, by voltage limiting mode, adjusts $P_l + P_{pv} = P_o$	charged by PV unit, fully charged, in floating charging

energy is transferred from the PV array and the voltage balancer to the dc bus, whereas various loads extract energy from the bus by converters. At the same time, batteries play an important role in compensating and balancing the difference between the PV array, voltage balancer, and loads through a bidirectional dc-dc converter. Considering the intermittency in power generated by the PV arrays due to the environmental change and the bidirectional power supplied by batteries, there are several possible operating modes for each group. In the following description, P_{pv} denotes the power generated by the PV array, P_1 denotes the power generated by the voltage balancer, and P_o denotes the power consumed by the load. The various modes are shown in Table II.

As mentioned in Table II, there are several operation modes due to different power flows and environmental uncertainty in each group. When the operation modes of the three groups are considered all together, the complexity will be significantly increased.

To make a simplification, the generalized voltage source (GVS) and generalized current source (GCS) are used to describe the bipolar dc microgrid: GVS refers to a subsystem that controls or affects its bus-side-port-voltage; and GCS refers to a subsystem that controls or affects its bus-side-port-current. The small-signal Thevenin equivalent circuit and Norton equivalent circuit for GVS and GCS are shown in Fig. 5. To describe the system by a standard form regardless of its operating modes as well as simplify the analysis, equivalent forms for three groups in bipolar dc microgrid are arranged. It should be noted that the small-signal model for the converter considers the full order for the power stage and the control loop instead of reducing the order. Therefore, the input admittance Y_i and the output

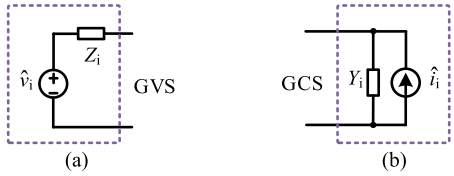

Fig. 5. Equivalent circuits: (a) Thevenin equivalent circuit for GVS and (b) Norton equivalent circuit for GCS.

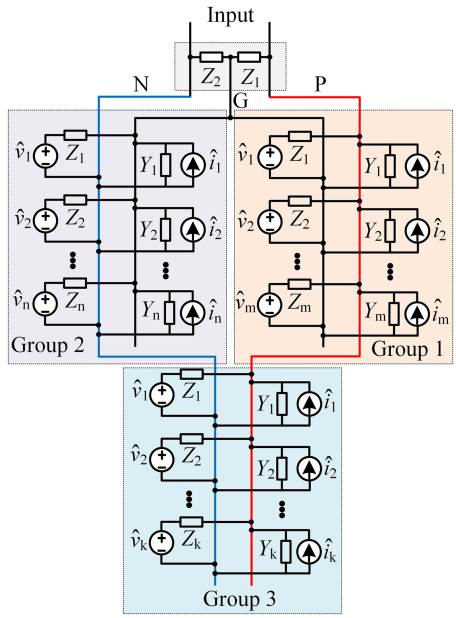

Fig. 6. Basic form of the bipolar DC microgrid.

impedance Z_i contain the accuracy and dominant frequency modes of a detailed converter.

According to the control objectives of converters with FCs or wind turbines, the different operations of bipolar dc microgrids can be classified. The converters with FCs or wind turbines are represented by the GVS and GCS. Using the stability conditions in the manuscript, the stability of bipolar dc microgrids with FCs or wind turbines can be investigated.

In a bipolar dc microgrid, the buck/boost topology is widely used as the voltage balancer, which can be expressed by two impedances Z_1 and Z_2. As a result, the bipolar dc microgrid can be represented by a basic form, as depicted in Fig. 6.

It should be noted that for bipolar dc microgrid, group 3 is connected directly with the input and the two wires are distributed to the other two groups respectively, which will consequently affect their operation. Moreover, groups 1 and 2 will have interactions with each other because they are connected by a voltage balancer.

III. STABILITY ASSESSMENT OF THE BIPOLAR DC MICROGRID

A. Simplification of the Bipolar DC Microgrid

As can be seen from Fig. 6, there are two parts for each group, consisting of the GVS part represented by Thevenin equivalent circuits and the GCS part represented by Norton

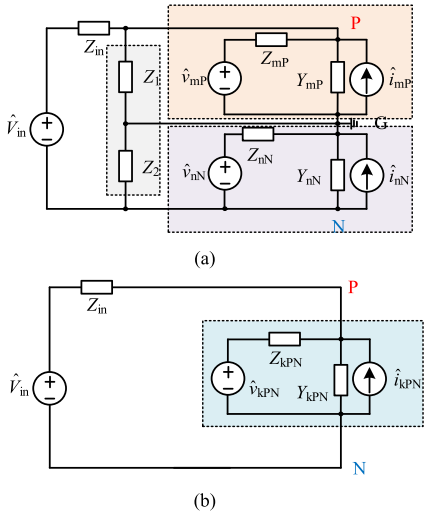

Fig. 7. Simplified form of the bipolar DC microgrid. (a) PG and GN bus ports. (b) GN bus port.

equivalent circuits. For further simplification, these two parts are combined separately. To analyze the characteristics of each bus port, based on their connection described in Figs. 4 and 5, the simplified form of bus port PG and GN are shown in Fig. 7(a), and the bus port PN are shown in Fig. 7(b). In Fig. 7, $\hat{V}_{\rm in}$ and $Z_{\rm in}$ are the input voltage and input impedance of the whole system. It can be seen in Fig. 7(a) and (b) that three groups in Fig. 7 are simplified into three compact three groups, where the impedances, admittances, voltages, and currents for the bus ports PG, GN, and PN, respectively, can be expressed as

$$\begin{cases} Z_{\rm mp} = Z_1||Z_2||\cdots||Z_{\rm m} \\ Y_{\rm mp} = \sum_{i=1}^{\rm m} Y_i \end{cases}, \begin{cases} \hat{v}_{\rm mP} = \frac{\sum_{i=1}^{\rm m} \frac{\hat{v}_i}{Z_i}}{\sum_{i=1}^{\rm m} \frac{1}{Z_i}} \\ \hat{i}_{\rm mP} = \sum_{i=1}^{\rm m} \hat{i}_i \end{cases} \tag{1}$$

$$\begin{cases} Z_{\rm nN} = Z_1||Z_2||\cdots||Z_{\rm n} \\ Y_{\rm nN} = \sum_{i=1}^{\rm n} Y_i \end{cases}, \begin{cases} \hat{v}_{\rm nP} = \frac{\sum_{i=1}^{\rm n} \frac{\hat{v}_i}{Z_i}}{\sum_{i=1}^{\rm n} \frac{1}{Z_i}} \\ \hat{i}_{\rm mP} = \sum_{i=1}^{\rm n} \hat{i}_i \end{cases} \tag{2}$$

$$\begin{cases} Z_{\rm kPN} = Z_1||Z_2||\cdots||Z_{\rm k} \\ Y_{\rm kPN} = \sum_{i=1}^{\rm k} Y_i \end{cases}, \begin{cases} \hat{v}_{\rm kNP} = \frac{\sum_{i=1}^{\rm k} \frac{\hat{v}_i}{Z_i}}{\sum_{i=1}^{\rm k} \frac{1}{Z_i}} \\ \hat{i}_{\rm mP} = \sum_{i=1}^{\rm k} \hat{i}_i \end{cases}. \tag{3}$$

As can be seen from Fig. 7(a) and (b) that the characteristics of the bus ports PG, GN, and PN can be obtained separately, where the stability for bus ports PG and GN may have interactions with each other because they are connected by the voltage balancer. To evaluate the stability of bus port PG, the bus port PG is looked into while the bus-port GN should be further equivalenced. At the same time, bus port PG should be further simplified if the stability of bus port GN is analyzed. Fig. 8 shows the corresponding equivalent process, where the impedances, admittances, voltages, and currents are expressed as

$$\begin{cases} Z'_{\rm nN} = \frac{Z_2}{1+Z_2 Y_{\rm nN}}||Z_{\rm nN} \\ \hat{v}'_{\rm nN} = \frac{\frac{Z_2}{1+Z_2 Y_{\rm nN}}\hat{v}_{\rm nN} + Z_{\rm nN}\hat{i}_{\rm nN}\left(\frac{1}{Z_2}+Y_{\rm nN}\right)}{\frac{Z_2}{1+Z_2 Y_{\rm nN}}+Z_{\rm nN}} \end{cases} \tag{4}$$

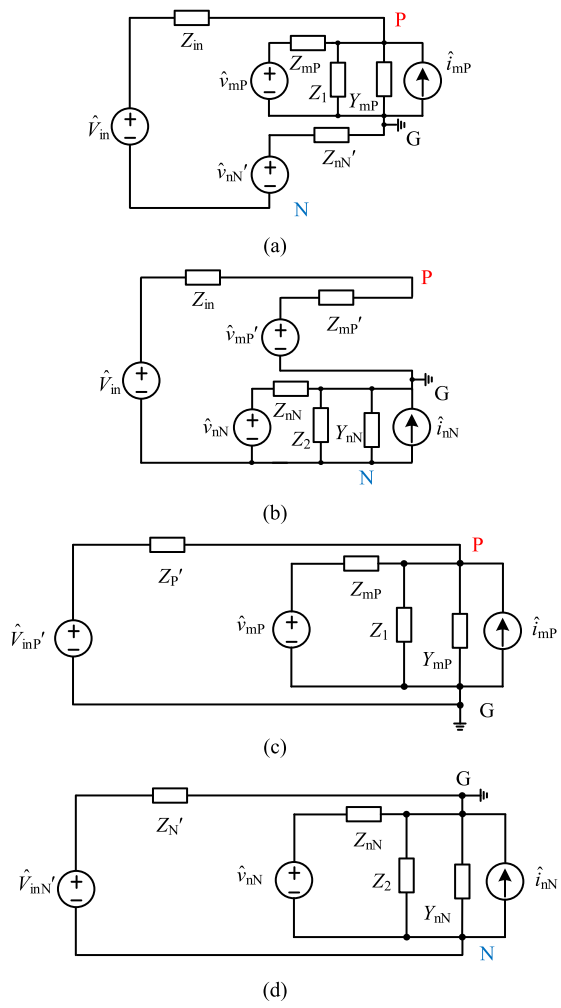

Fig. 8. Further simplification of the bipolar DC microgrid. (a) Simplification of the bus port PG. (b) Bus port GN. (c) System looked into bus port PG. (d) System looked into bus port GN.

$$\begin{cases} Z'_{\rm mP} = \frac{Z_1}{1+Z_1 Y_{\rm mP}}||Z_{\rm mP} \\ \hat{v}'_{\rm mP} = \frac{\frac{Z_1}{1+Z_1 Y_{\rm mP}}\hat{v}_{\rm mP} + Z_{\rm mP}\hat{i}_{\rm mP}\left(\frac{1}{Z_1}+Y_{\rm mP}\right)}{\frac{Z_1}{1+Z_1 Y_{\rm mP}}+Z_{\rm mP}} \end{cases} \tag{5}$$

$$\begin{cases} Z'_{\rm P} = Z'_{\rm nN} + Z_{\rm in} \\ \hat{V}'_{\rm inP} = \hat{V}_{\rm in} + \hat{v}'_{\rm nN} \end{cases} \tag{6}$$

$$\begin{cases} Z'_{\rm N} = Z'_{\rm mP} + Z_{\rm in} \\ \hat{V}'_{\rm inN} = \hat{V}_{\rm in} + \hat{v}'_{\rm mP} \end{cases} \tag{7}$$

$$\begin{cases} Z''_{\rm mP} = Z_{\rm mP}||Z'_{\rm P}, Y''_{\rm mP} = \frac{1}{Z_1} + Y_{\rm mP} \\ \hat{v}''_{\rm mP} = \frac{Z_{\rm mP}}{Z_{\rm mP}+Z'_{\rm P}}\hat{V}'_{\rm inP} + \frac{Z'_{\rm P}}{Z_{\rm mP}+Z'_{\rm P}}\hat{v}_{\rm mP} \end{cases} \tag{8}$$

$$\begin{cases} Z''_{\rm nN} = Z_{\rm nN}||Z'_{\rm N}, Y''_{\rm nN} = \frac{1}{Z_2} + Y_{\rm nN} \\ \hat{v}''_{\rm nN} = \frac{Z_{\rm nN}}{Z_{\rm nN}+Z'_{\rm N}}\hat{V}'_{\rm inN} + \frac{Z'_{\rm N}}{Z_{\rm nN}+Z'_{\rm N}}\hat{v}_{\rm nN} \end{cases} \tag{9}$$

$$\begin{cases} Z'_{\rm kPN} = Z_{\rm kPN}||Z_{\rm in} \\ \hat{v}'_{\rm kNP} = \frac{Z_{\rm kPN}}{Z_{\rm kPN}+Z_{\rm in}}\hat{V}_{\rm in} + \frac{Z_{\rm in}}{Z_{\rm kPN}+Z_{\rm in}}\hat{v}_{\rm kNP} \end{cases}. \tag{10}$$

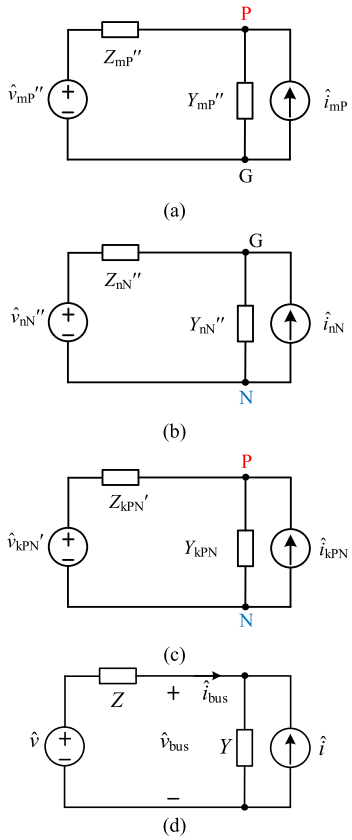

Fig. 9. Three concise groups including three bus ports and general structure. (a) PG bus port. (b) GN bus port. (c) PN bus port. (d) General structure.

Then, the bipolar dc microgrid can be simplified into three more concise groups including three bus ports, PG, GN, and PN, as shown in Fig. 9. Different bus ports share the same equivalent circuit form with each other and the general structure is presented in Fig. 9(d). As a result, the stability of the bipolar dc microgrid can be analyzed by assessing the stability of the three groups.

B. Stability Analysis

It can be seen from Fig. 9, the bipolar dc microgrid can be simplified as three concise groups which have the same structures. Assuming a general expression for the impedance, admittance, voltage, and current in Fig. 9, denoted as Z, Y, $\hat{v}$, and $\hat{i}$, the bus voltage $\hat{v}_{bus}$ and bus current $\hat{i}_{bus}$ can be obtained as

$$\begin{cases} \hat{v}_{bus} = \frac{1}{1+ZY}\hat{v} + \frac{Z}{1+ZY}\hat{i} \\ \hat{i}_{bus} = \frac{Y}{1+ZY}\hat{v} - \frac{1}{1+ZY}\hat{i} \end{cases}. \tag{11}$$

To make the system stable, the condition of having no right-half-plane poles in (11) should be satisfied. Using fractions to denote Z and Y: $Z = N_Z/D_Z$, $Y = D_Y/N_Y$, we get

$$\begin{cases} \frac{1}{1+ZY} = \frac{N_Y D_Z}{N_Y D_Z + D_Y N_Z} \\ \frac{Z}{1+ZY} = \frac{N_Z N_Y}{N_Y D_Z + D_Y N_Z} \\ \frac{Y}{1+ZY} = \frac{D_Z D_Y}{N_Y D_Z + D_Y N_Z} \end{cases}. \tag{12}$$

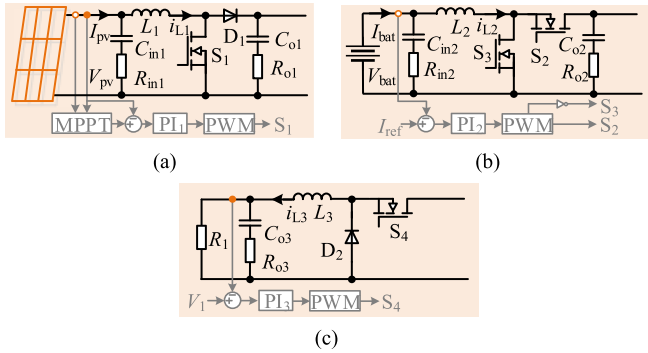

Fig. 10. Applied basic units in the system. (a) PV unit. (b) Energy storage unit. (c) Load unit.

TABLE III
PARAMETERS OF THE SYSTEM

PV unit	**Parameters**	L_1	C_{in1}	R_{in1}	C_{o1}	R_{o1}	V_{MPPT}
	Values	100μH	100μF	0.1Ω	100μF	0.1Ω	17V
Energy storage unit	**Parameters**	L_2	C_{in2}	R_{in2}	C_{o2}	R_{o2}	V_{bat}
	Values	100μH	100μF	0.1Ω	100μF	0.1Ω	12V
Load unit	**Parameters**	V_{PG}	L_3	C_{o3}	R_{o3}	V_{NG}	V_{PN}
	Values	24V	100μH	100μF	0.1Ω	-24V	48V

As it can be seen, expressions in (12) share the same denominators, which means if $(1+ZY)$ does not have any right-half-plane zeros, the system will be stable without having restrictions of right-half-plane zero or pole on Z or Y. Therefore, the stability of the bipolar dc microgrid can be adjudged by the following two conditions.

Condition 1: The number of right-half-plane zeros for PN bus port satisfies

$$\mathrm{RHZ}\left(1 + Z'_{kPN}Y_{kPN}\right) = 0. \tag{13}$$

Condition 2: The number of right-half-plane zeros for the PG bus port and GN bus port satisfies

$$\begin{cases} \mathrm{RHZ}\left(1 + Z_{mP}''Y_{mP}''\right) = 0 \\ \mathrm{RHZ}\left(1 + Z_{nN}''Y_{nN}''\right) = 0 \end{cases}. \tag{14}$$

Condition 1 can be used to test the stability of the PN bus port. Only if condition 1 is satisfied, condition 2 is adopted to assess the stability of the PG bus port and the GN bus port because their inputs are affected by the PN bus port.

According to (14), since Z_{nN}'' and Z_{mP}'' both include information of the bus ports PG and GN, the interactions of these two buses can be revealed. Moreover, the stability of different bus ports in bipolar dc microgrid can be investigated, providing criteria from a point of separate way.

IV. Case Study

Case studies are conducted to illustrate the stability issues for bipolar dc microgrids as well as verify the aforementioned stability conditions. Fig. 10 shows the basic units used in the studied system. For each unit, parameters are provided in Table III.

Three cases are presented: Case 1 investigates the bipolar dc microgrid only connected with loads, and the system is shown in

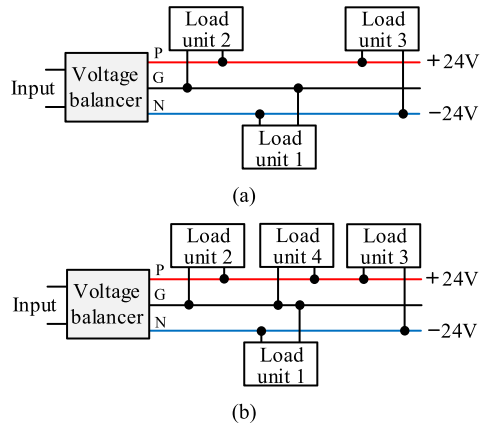

Fig. 11. Case 1. (a) Bipolar DC microgrid with the same number of load units connected to each bus port. (b) Bipolar DC microgrid with a different number of load units connected to each bus port.

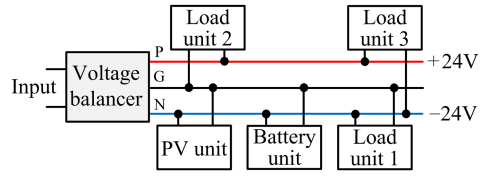

Fig. 12. Case 2.

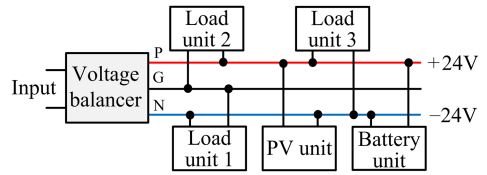

Fig. 13. Case 3.

Fig. 11; based on case 1, case 2 studies the system with a PV unit and energy storage unit to the GN bus port, as shown in Fig. 12; based on case 1, case 3 studies the system with connecting a PV unit and energy storage unit to the PN bus port, as shown in Fig. 13. It should be noted that for all the cases, a voltage source with *LC* filter is used as the input and the widely applied buck/boost topology is used as the voltage balancer. Load unit 1, load unit 2, load unit 3, and load unit 4 using the voltage control can be regarded as CPLs.

A. Case 1

The parameters $Z_{\mathrm{mP}}{}''Y_{\mathrm{mP}}{}''$ for the PG bus port, $Z_{\mathrm{nN}}{}''Y_{\mathrm{nN}}{}''$ for the GN bus port, and $Z_{\mathrm{kPN}}{}'Y_{\mathrm{kPN}}$ for the PN bus port in case 1(a) can be expressed as

$$\begin{cases} 1+Z_{\mathrm{mP}}{}''Y_{\mathrm{mP}}{}''=1+\left(\frac{1}{Z_1}+Y_{\mathrm{L2}}\right)\left(Z_{\mathrm{LC}}+\frac{Z_2}{1+Z_2Y_{\mathrm{L1}}}\right) \\ 1+Z_{\mathrm{nN}}{}''Y_{\mathrm{nN}}{}''=1+\left(\frac{1}{Z_2}+Y_{\mathrm{L1}}\right)\left(Z_{\mathrm{LC}}+\frac{Z_1}{1+Z_1Y_{\mathrm{L2}}}\right) \\ 1+Z'_{\mathrm{kPN}}Y_{\mathrm{kPN}}=1+Z_{\mathrm{LC}}Y_{\mathrm{L3}} \end{cases} \tag{15}$$

where Y_{L1}, Y_{L2}, and Y_{L3} are the admittances of the load units: load unit 1, load unit 2, and load unit 3, respectively; Z_1 and Z_2 are the impedances of the voltage balancer, which can be derived based on small signal models [20], [26]. It should be noted that the specific expressions of the impedance models are different with various controls while they can be classified as GVS and GCS represented by Thevenin equivalent circuit and the Norton equivalent circuit. Therefore, the proposed stability assessment method has no limitation for the converters with different controls if their output impedance or input admittance can be derived.

The stability of the system in case 1(a) can be analyzed by mapping the pole-zero characteristics of (15). To test the interactions between different bus ports, loads and reference voltages are varied, and the pole-zero maps for the PG and GN bus port are shown in Fig. 14, where R_{11}, R_{12}, and R_{13} are the loads, and V_{11}, V_{12}, and V_{13} are the reference voltages of load unit 1, 2, and 3, respectively. In Fig. 14, $R_{13}=10\ \Omega$ and $V_{13}=12$ V are chosen for load unit 3 connected to the PN bus port. Moreover, when $R_{11}=R_{12}=10\ \Omega$ and $V_{11}=V_{12}=V_{13}=12$ V, the pole-zero maps for the PN bus port with different R_{13} are shown in Fig. 15.

As can be seen from Figs. 14 and 15(a), with $R_{13}=10\ \Omega$ and $V_{13}=12$ V, RHZ $(1+Z_{\mathrm{kPN}}{}'Y_{\mathrm{kPN}})$ equals 0, which means that the PN bus port is stable. Under this condition, when R_1 and R_2, or V_{11} and V_{12} are different, condition 2 in (14) is not met, indicating that the bus voltages of the PG bus port and GN bus port are unstable with unbalanced load units. When $R_{13}=2\ \Omega$ and $V_{13}=12$ V, RHZ $(1+Z_{\mathrm{kPN}}{}'Y_{\mathrm{kPN}})=0$ is not satisfied, demonstrating the instability issue of the PN bus port. Since condition 1 in (13) is not satisfied, according to the stability assessment method, instability phenomena will appear in the PG and GN bus ports.

Selecting $R_{13}=10\ \Omega$ and $V_{13}=12$ V, Fig. 16 shows the pole-zero maps of another unbalanced situation by connecting two load units to the PG bus port and one load unit to the GN bus port, as shown in case 1 (b). $Z_{\mathrm{mP}}{}''Y_{\mathrm{mP}}$" for the PG bus port, $Z_{\mathrm{nN}}{}''Y_{\mathrm{nN}}$" for the GN bus port, and $Z_{\mathrm{kPN}}{}'Y_{\mathrm{kPN}}$ for the PN bus port in case 1(b) can be expressed as

$$\begin{cases} 1+Z_{\mathrm{mP}}{}''Y_{\mathrm{mP}}{}''=1+\left(\frac{1}{Z_1}+Y_{\mathrm{L4}}+Y_{\mathrm{L2}}\right)\left(Z_{\mathrm{LC}}+\frac{Z_2}{1+Z_2Y_{\mathrm{L1}}}\right) \\ 1+Z_{\mathrm{nN}}{}''Y_{\mathrm{nN}}{}''=1+\left(\frac{1}{Z_2}+Y_{\mathrm{L1}}\right)\left(Z_{\mathrm{LC}}+\frac{Z_1}{1+Z_1Y_{\mathrm{L2}}+Z_1Y_{\mathrm{L4}}}\right) \\ 1+Z'_{\mathrm{kPN}}Y_{\mathrm{kPN}}=1+Z_{\mathrm{LC}}Y_{\mathrm{L3}} \end{cases} \tag{16}$$

where Y_{L4} is the admittance of load unit 4.

It can be observed from Fig. 16 that when a different number of load units are connected to the bipolar bus ports, condition 2 in (14) is not met. Therefore, the bus voltages of both PG and the GN bus ports are unstable.

To verify the stability conditions, an experimental set-up for case 1 is shown in Fig. 17, where the load unit shown in Fig. 10(c) is used as the load; the control system is implemented in the DSP (TMS320F28335). The experimental waveforms

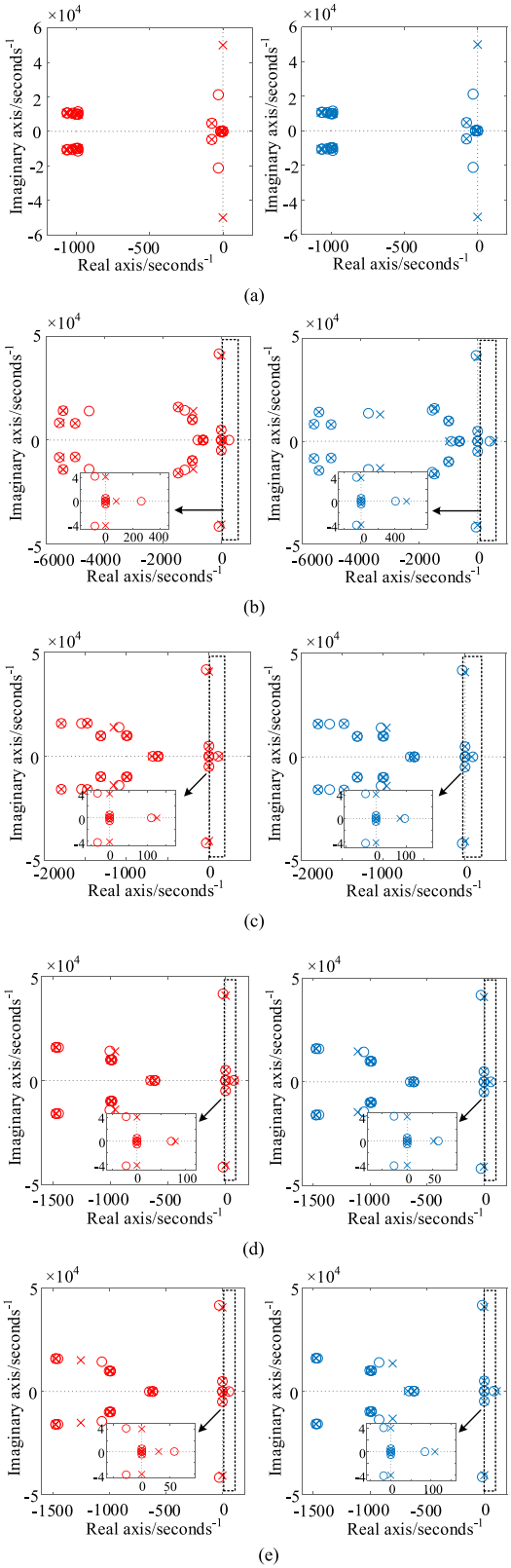

Fig. 14. Pole-zero maps for the PG bus port and GN bus port expressed in (15) under different parameters. (a) $R_{11} = 10\ \Omega$ and $R_{12} = 10\ \Omega$. (b) $R_{11} = 2\ \Omega$ and $R_{12} = 10\ \Omega$. (c) $R_{11} = 10\ \Omega$ and $R_{12} = 5\ \Omega$. (d) $V_{11} = 10$ V and $V_{12} = 12$ V. (e) $V_{11} = 12$ V and $V_{12} = 6$ V.

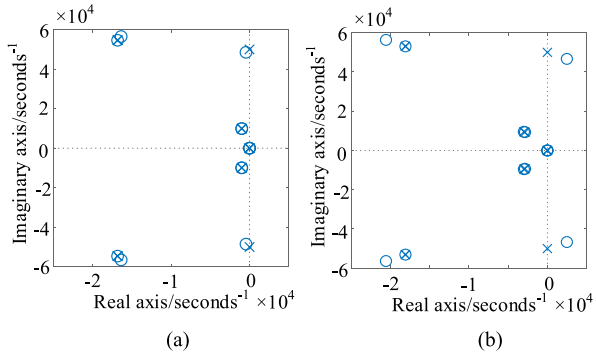

Fig. 15. Pole-zero maps for the PN bus port. (a) $R_{13} = 10\ \Omega$ and $V_{13} = 12$ V. (b) $R_{13} = 2\ \Omega$ and $V_{13} = 12$ V.

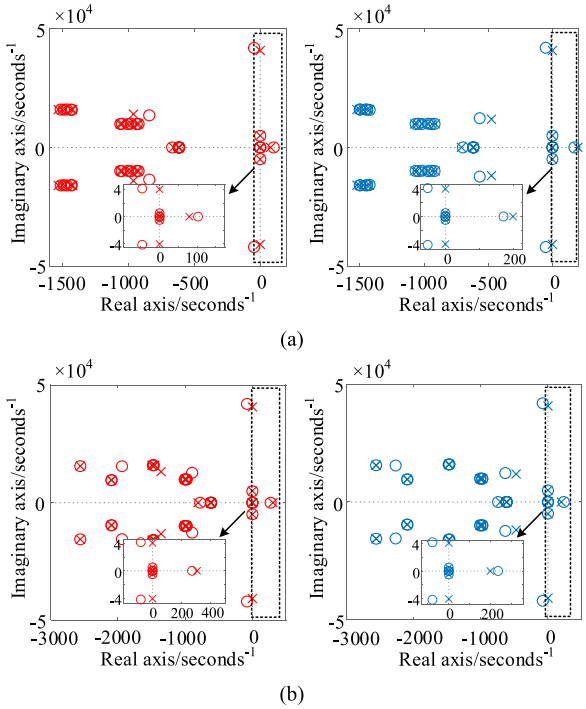

Fig. 16. Pole-zero maps for PG bus port and GN bus port expressed in (16) under $R_{11} = R_{12} = R_{13} = 10\ \Omega$ and $V_{11} = V_{12} = V_{13} = 12$ V. (a) $R_{14} = 10\ \Omega$. (b) $R_{14} = 5\ \Omega$.

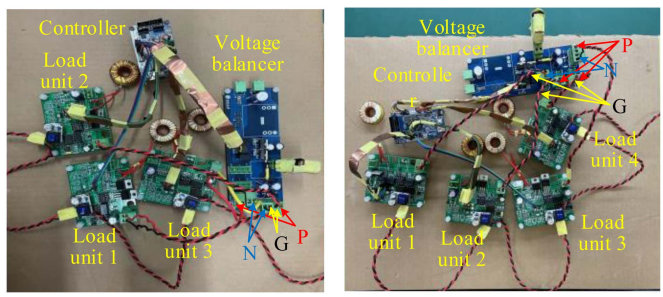

Fig. 17. Experimental set-up for case 1. (a) Case 1(a). (b) Case 1(b).

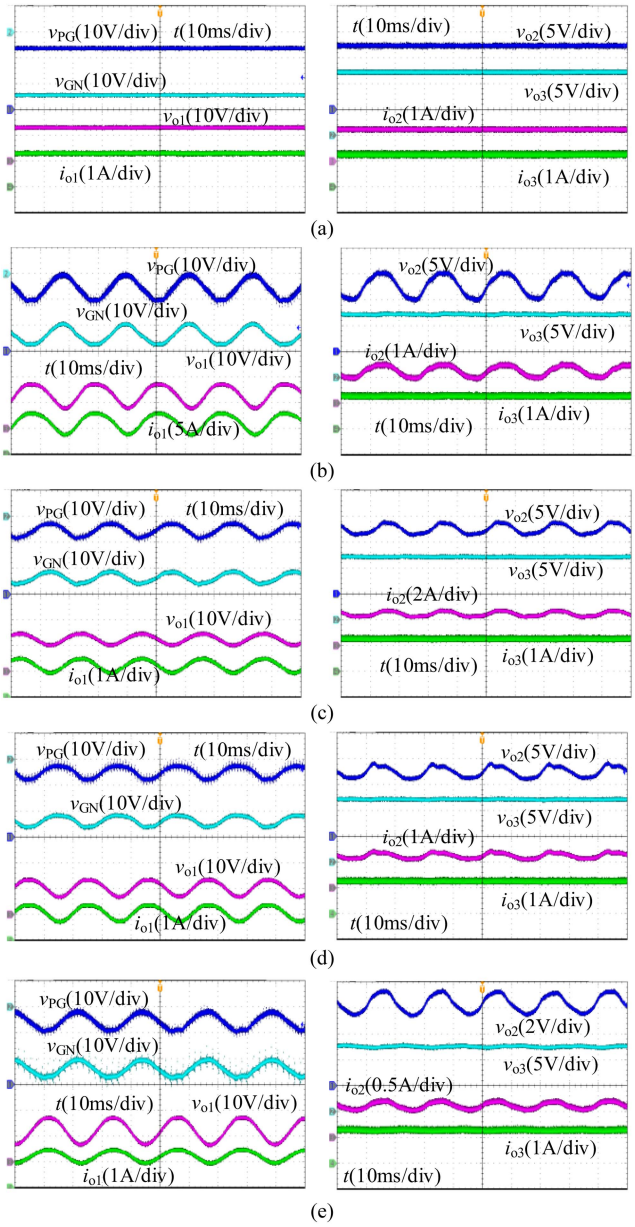

Fig. 18. Experimental waveforms for case 1 (a). (a) $R_{11} = 10\ \Omega$ and $R_{12} = 10\ \Omega$. (b) $R_{11} = 2\ \Omega$ and $R_{12} = 10\ \Omega$. (c) $R_{11} = 10\ \Omega$ and $R_{12} = 5\ \Omega$. (d) $V_{11} = 10$ V and $V_{12} = 12$ V. (e) $V_{11} = 12$ V and $V_{12} = 6$ V.

of case 1(a) and case 1(b) are presented in Figs. 18 and 19, respectively.

In Fig. 18, voltages of PG and GN bus ports are stable when $R_{13} = R_{12} = 10\ \Omega$. Both the voltages of PG and GN bus ports are oscillated when $R_{11} = 2\ \Omega$, $R_{12} = 10\ \Omega$ or $R_{11} = 10\ \Omega$, $R_{12} = 5\ \Omega$ or $V_{11} = 10$ V, $V_{12} = 12$ V or $V_{11} = 12$ V, and $V_{12} = 6$ V, whereas the voltage of the load unit 3 connected to PN bus port is stable which means the voltage of bust port PN is stable.

In Fig. 19, oscillations exist in PG and GN bus port voltages as well as the voltages and currents of the load units 1, 2, and 4 connected to the PG or GN bus ports. But the voltage and the current of load unit 3 are stable which indicates a stable operation of the PN bus port. In summary, with relatively small load R or unbalanced load units connected to the symmetrical

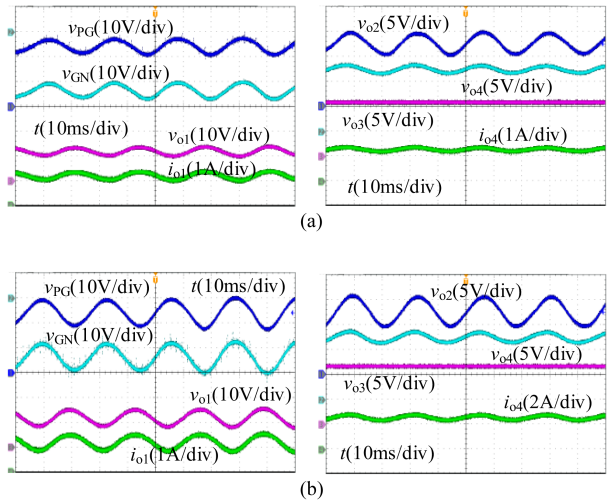

Fig. 19. Experimental waveforms for case 1 (b) under $R_{11} = R_{12} = R_{13} = 10\ \Omega$ and $V_{11} = V_{12} = V_{13} = 12$ V. (a) $R_{14} = 10\ \Omega$. (b) $R_{14} = 5\ \Omega$.

bus ports, the bipolar dc microgrid is more likely to be unstable. The oscillations in the PG and the GN bus ports have little influence on the PN bus port, while the stability of the PN bus port will affect both PG and GN bus ports. Finally, it can be confirmed from Figs. 14, 15, 18, and 19 that the experimental results validate the theoretical stability evaluation studies.

B. Case 2

To investigate the effect of the PV unit and energy storage unit on the stability of a bipolar dc microgrid with unbalanced loads connected to the symmetrical bus ports, case 2 is hereby studied. $Z_{\mathrm{mP}}{}''Y_{\mathrm{mP}}{}''$ for PG bus port, $Z_{\mathrm{nN}}{}''Y_{\mathrm{nN}}{}''$ for GN bus port, $Z_{\mathrm{kPN}}{}'Y_{\mathrm{kPN}}$ for PN bus port can be expressed as follows:

$$\begin{cases} 1 + Z_{\mathrm{mP}}{}''Y_{\mathrm{mP}}{}'' = 1 + \left(\frac{1}{Z_1} + Y_{\mathrm{L2}}\right) \\ \quad \times \left(Z_{\mathrm{LC}} + \frac{Z_2}{1+Z_2(Y_{\mathrm{L1}}+Y_{\mathrm{pv}}+Y_{\mathrm{ba}})}\right) \\ 1 + Z_{\mathrm{nN}}{}''Y_{\mathrm{nN}}{}'' = 1 + \left(\frac{1}{Z_2} + Y_{\mathrm{L1}} + Y_{\mathrm{pv}} + Y_{\mathrm{ba}}\right) \\ \quad \times \left(Z_{\mathrm{LC}} + \frac{Z_1}{1+Z_1 Y_{\mathrm{L2}}}\right) \\ 1 + Z'_{\mathrm{kPN}}Y_{\mathrm{kPN}} = 1 + Z_{\mathrm{LC}}Y_{\mathrm{L3}} \end{cases} \tag{17}$$

where Y_{pv} and Y_{ba} are the admittances of the PV unit and the energy storage unit.

The pole-zero maps for the PG bus port and the GN bus port with PV unit or energy storage unit expressed in (17) are shown in Figs. 20 and 21, respectively. The experimental setup is shown in Fig. 22.

The experimental results in Figs. 23 and 24 indicate that in a bipolar dc microgrid with unbalanced load units connected to symmetrical bus ports, the linking of the PV unit can improve the stability when there is a relatively small difference between the two unbalanced load units. When the difference between the two unbalanced load units is relatively large, i.e., $R_{11} = 2\ \Omega$ and $R_{12} = 10\ \Omega$, there is right-half-plane zero in Fig. 20(b), indicating that the linking of the PV unit fails to stabilize the system. With the connection of the PV unit and energy storage unit to the

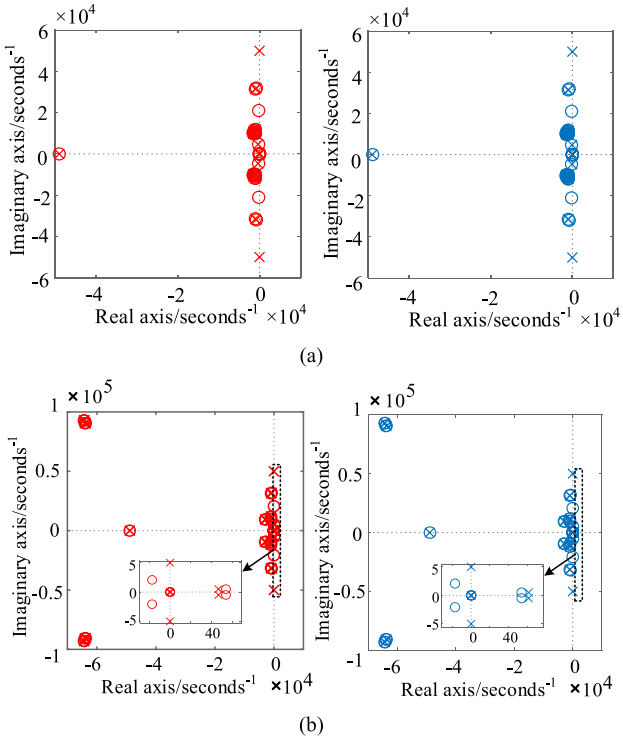

Fig. 20. Pole-zero maps for PG bus port and GN bus port when GN bus port is connected with PV unit. (a) $R_{11} = 5\ \Omega$ and $R_{12} = 10\ \Omega$. (b) $R_{11} = 2\ \Omega$ and $R_{12} = 10\ \Omega$.

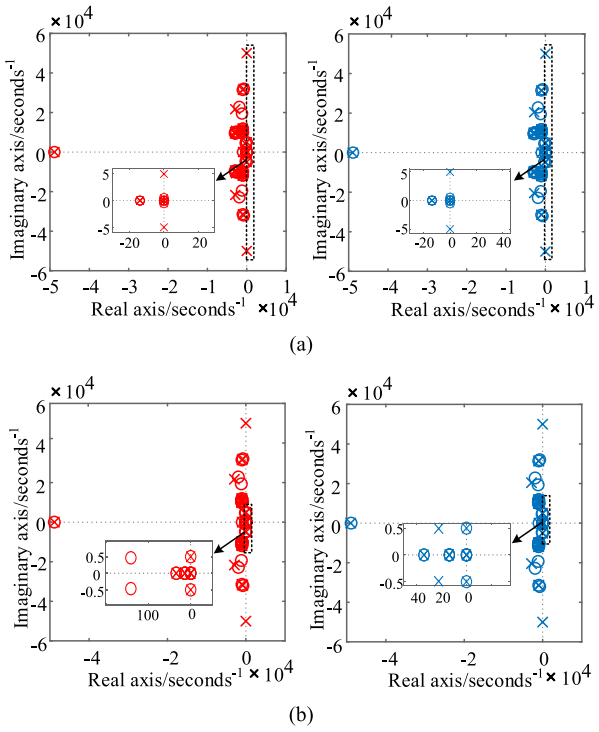

Fig. 21. Pole-zero maps for PG bus port and GN bus port when GN bus port is connected with PV unit and energy storage unit. (a) $R_{11} = 2\ \Omega$ and $R_{12} = 10\ \Omega$. (b) $V_{11} = 12$ V and $V_{12} = 6$ V.

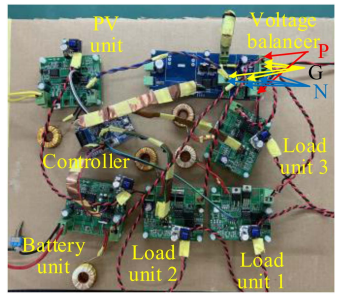

Fig. 22. Experimental set-up for case 2.

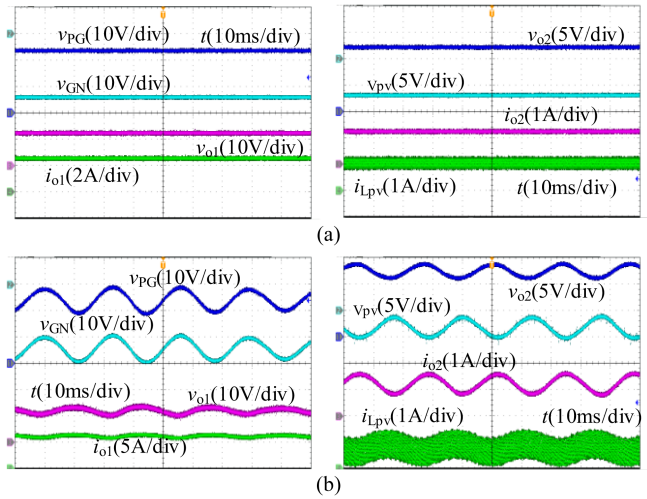

Fig. 23. Experimental waveforms for the system when GN bus port is connected with the PV unit. (a) $R_{11} = 5\ \Omega$ and $R_{12} = 10\ \Omega$. (b) $R_{11} = 2\ \Omega$ and $R_{12} = 10\ \Omega$.

GN bus port, there is no right-half-plane zero in Fig. 21(a), which means the bipolar dc microgrid operates stably. Moreover, when $R_{11} = 10\ \Omega$ and $R_{12} = 10\ \Omega$, oscillations are caused by unbalanced loads due to different reference voltages, i.e., $V_{11} = 12$ V and $V_{12} = 6$ V, can be also eliminated by connecting the PV unit and energy storage unit to one of the symmetrical bus ports.

C. Case 3

Case 3 is used to investigate the stability of the PN bus port in a bipolar dc microgrid. $Z_{\mathrm{mP}}{}''Y_{\mathrm{mP}}$" for PG bus port, $Z_{\mathrm{nN}}{}''Y_{\mathrm{nN}}$" for GN bus port, $Z_{\mathrm{kPN}}{}'Y_{\mathrm{kPN}}$ for PN bus port can be expressed as

$$\begin{cases} 1 + Z_{\mathrm{mP}}{}''Y_{\mathrm{mP}}{}'' = 1 + \left(\frac{1}{Z_1} + Y_{\mathrm{L2}}\right)\left(Z_{\mathrm{LC}} + \frac{Z_2}{1+Z_2Y_{\mathrm{L1}}}\right) \\ 1 + Z_{\mathrm{nN}}{}''Y_{\mathrm{nN}}{}'' = 1 + \left(\frac{1}{Z_2} + Y_{\mathrm{L1}}\right)\left(Z_{\mathrm{LC}} + \frac{Z_1}{1+Z_1Y_{\mathrm{L2}}}\right) \\ 1 + Z'_{\mathrm{kPN}}Y_{\mathrm{kPN}} = 1 + Z_{\mathrm{LC}}\left(Y_{\mathrm{L}}3 + Y_{\mathrm{pv}} + Y_{\mathrm{ba}}\right) \end{cases} . \tag{18}$$

With the PV unit connected to the PN bus port, pole-zero maps for the PN bus port with $R_{13} = 5\ \Omega$ and $R_{13} = 2\ \Omega$ are shown in Fig. 25(a) and (b), whereas Fig. 25(c) shows the pole-zero

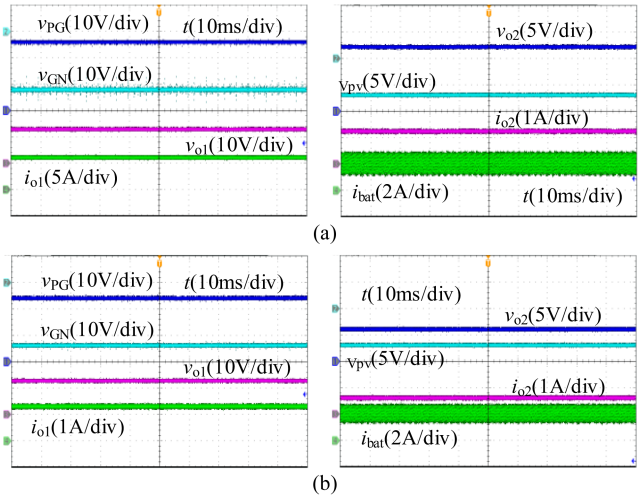

Fig. 24. Experimental waveforms for the system when GN bus port is connected with the PV unit and energy storage unit. (a) $R_{11} = 2\ \Omega$ and $R_{12} = 10\ \Omega$. (b) $V_{11} = 12$ V and $V_{12} = 6$ V.

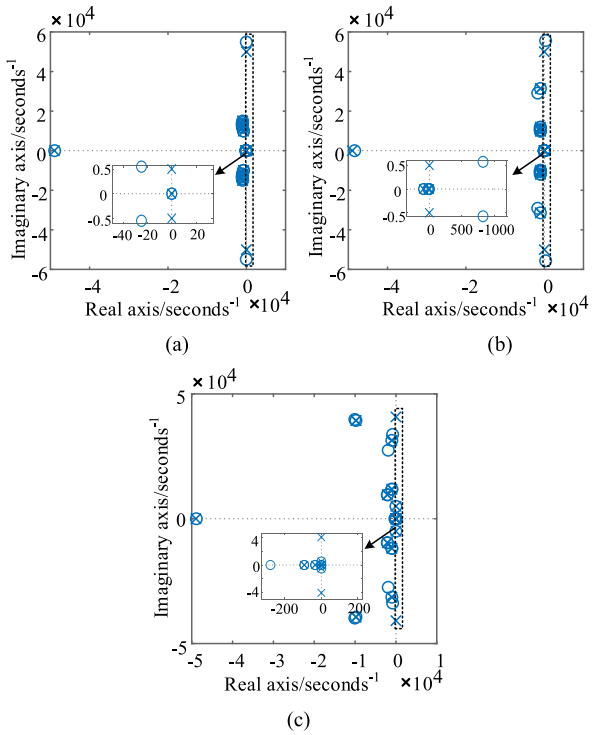

Fig. 25. Pole-zero maps for the PN bus port. (a) $R_{13} = 5\ \Omega$ with PV unit. (b) $R_{13} = 2\ \Omega$ with PV unit. (c) $R_{13} = 2\ \Omega$ with PV unit and energy storage unit.

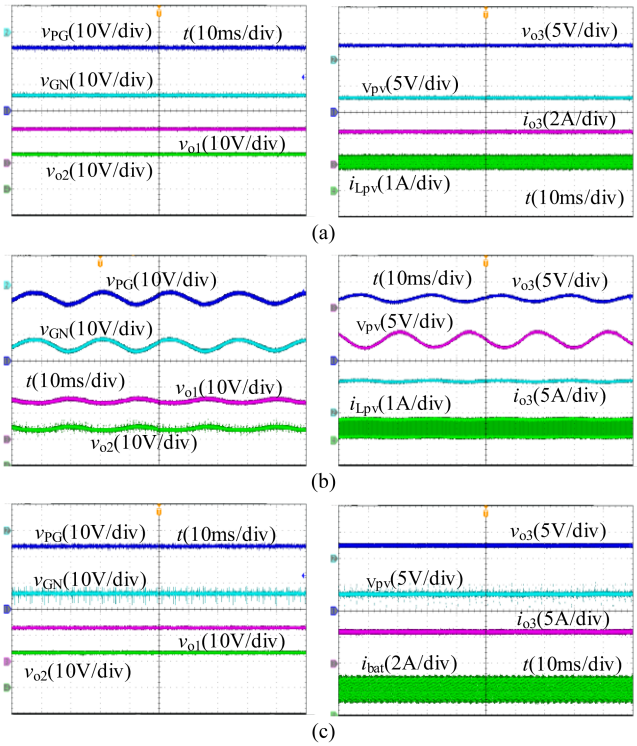

Fig. 26. Experimental waveforms for the system. (a) $R_{13} = 5\ \Omega$ with PV unit. (b) $R_{13} = 2\ \Omega$ with PV unit. (c) $R_{13} = 2\ \Omega$ with PV unit and energy storage unit.

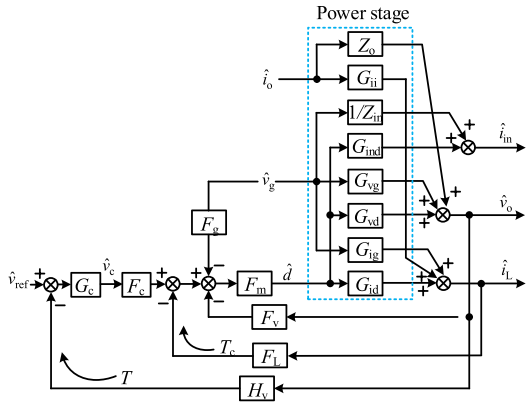

Fig. 27. General small signal model for a converter.

maps for the PN bus port with $R_{13} = 2\Omega$ with both the PV unit and energy storage unit connected. As it can be seen, the right-half-plane zeros in (15) can be shifted to the left half-plane due to the connection of the PV unit and energy storage unit which indicates that the bus voltage of the PN bus port is stable.

Connecting the PV unit and battery unit to the PN bus port, the experimental set-up is similar to that shown in Fig. 22. From the experimental results in Fig. 26, it can be concluded that connecting the PV unit to the PN bus port will make the system stable to some extent. However, there are large oscillations in the PN bus port which also causes instabilities in the PG bus port and the GN bus port when $R_{13} = 2\ \Omega$. By linking the PV unit and energy storage unit to the PN bus port, instabilities will be reduced.

The detailed summaries of the above cases are given in Table IV, which reveal the stability interactions among three bus ports and address the stability issues in bipolar dc, microgrid.

TABLE IV
SUMMARY OF THE CASES

Cases	Parameters	PG	GN	PN
Case 1 (a):load unit 1 connected to GN bus port, load unit 2 connected to PG bus port, load unit 3 connected to PN bus port	$R_{l1} = 10\ \Omega$, $R_{l2} = 10\ \Omega$	Stable	Stable	Stable
	$R_{l1} = 2\ \Omega$, $R_{l2} = 10\ \Omega$	Unstable	Unstable	Stable
	$R_{l1} = 10\ \Omega$, $R_{l2} = 5\ \Omega$	Unstable	Unstable	Stable
	$V_{l1} = 10$ V, $V_{l2} = 12$ V	Unstable	Unstable	Stable
	$V_{l1} = 12$ V, $V_{l2} = 6$ V	Unstable	Unstable	Stable
Case 1 (b): additional load unit 4 connected to PG bus port	$R_{l4} = 10\ \Omega$	Unstable	Unstable	Stable
	$R_{l4} = 5\ \Omega$	Unstable	Unstable	Stable
Case 2: load unit 1 connected to GN bus port, load unit 2 connected to PG bus port, load unit 3 connected to PN bus port	$R_{l1} = 5\ \Omega$, $R_{l2} = 10\ \Omega$ (PV unit connected to GN bus port)	Stable	Stable	Stable
	$R_{l1} = 2\ \Omega$, $R_{l2} = 10\ \Omega$ (PV unit connected to GN bus port)	Unstable	Unstable	Stable
	$R_{l1} = 2\ \Omega$, $R_{l2} = 10\ \Omega$ (PV unit and battery unit connected to GN bus port)	Stable	Stable	Stable
	$V_{l1} = 12$ V, $V_{l2} = 6$ V (PV unit and battery unit connected to GN bus port)	Stable	Stable	Stable
Case 3: load unit 1 connected to GN bus port, load unit 2 connected to PG bus port, load unit 3 connected to PN bus port	$R_{l3} = 5\ \Omega$ (PV unit connected to PN bus port)	Stable	Stable	Stable
	$R_{l3} = 2\ \Omega$ (PV unit connected to PN bus port)	Unstable	Unstable	Unstable
	$R_{l3} = 2\ \Omega$ (PV unit and battery unit connected to PN bus port)	Stable	Stable	Stable

VI. CONCLUSION

This article proposes a stability assessment method for the bipolar dc microgrid based on its simplification forms. The stability issues of the bipolar dc microgrid and the mutual influence among different bus ports are investigated by three cases: 1) $\pm V_{\rm dc}$ bus ports are connected with balanced and unbalanced load units; 2) $-V_{\rm dc}$ bus port is connected with the PV unit and the energy storage unit; and 3) the $2V_{\rm dc}$ bus port is connected with the PV unit and the energy storage unit. Experimental results indicate the effectiveness of the proposed method. The novel features of this stability evaluation method can be concluded here as follows.

1) The stability interactions among three bus ports in a bipolar dc microgrid are revealed, which indicates that the oscillations in the PG bus port and GN bus port have little influence on the PN bus port, while the instabilities in the PN bus port will affect both the PG bus port and the GN bus port. Moreover, there are stable interactions between the PG bus port and the GN bus port.
2) The stability of the bipolar dc microgrid can be analyzed separately, which means the stability of each bus port can be evaluated respectively, being simple and easy to extend to plug-and-play applications and evaluate the stability of the complex system.
3) For a bipolar dc microgrid, if bus ports are connected only with load units, a relatively small load resistance may cause oscillations in bus voltages. Moreover, instability issues will exist if unbalanced load units are connected to the PG bus port and the GN bus port in the bipolar dc microgrid. It is suggested to introduce the PV unit and energy storage unit to improve the stability of the system.

APPENDIX

The derivation of the output impedances for the voltage balancer is the same as the conventional small signal model derivation. Fig. 27 shows a widely used small signal model for a converter, which contains the power stage and the control part. The state space average model and the time average equivalent circuit approach are efficient ways to derive the open-loop transfer function for the power stage.

A small-signal expression of the output voltage can be obtained according to the power stage transfer functions mentioned above

$$\widehat{v}_{\rm o}(s) = G_{\rm vd}(s)\widehat{d}(s) + G_{\rm vg}(s)\widehat{v}_{\rm g}(s) + Z_{\rm o}(s)\widehat{i}_{\rm o}(s). \tag{A1}$$

In Fig. 27, the small-signal expression of duty cycle d can be deduced based on the control method, and by introducing the small-signal perturbation and linearization.

According to Fig. 27, the inner-loop output impedance $Z_{\rm out}$ are derived as follows:

$$Z_{\rm out} = \frac{\widehat{v}_{\rm o}}{\widehat{i}_{\rm o}} = \frac{Z_{\rm o} + F_{\rm L}F_{\rm m}(G_{\rm id}Z_{\rm o} + G_{\rm ii}Z_{\rm vd})}{1 + F_{\rm L}F_{\rm m}G_{\rm id} + F_{\rm v}F_{\rm m}G_{\rm vd}} \tag{A2}$$

where $G_{\rm x} = F_{\rm m}F_{\rm L}(G_{\rm vd}G_{\rm id} - G_{\rm vd}G_{\rm ig})$.

The closed-loop output impedance $Z_{\rm i}$ can be given to express the performance of different control techniques

$$Z_{\rm i} = \frac{Z_{\rm out}}{1 + T_{\rm new}} \tag{A3}$$

where $T_{\rm new}(s) = G_{\rm c}G_{\rm vc}H_{\rm v}$ is the loop gain of the output voltage loop. As a result, Z_1 and Z_2 can be represented as: Z_1 and $Z_2 = Z_{\rm i}/2$.

It should be noted that the small signal model is general: by changing the coefficients in control ($F_{\rm g}, F_{\rm v}, F_{\rm c}, F_{\rm L}$) or changing the transfer function in the power stage, the output impedance of different converters with different controls can be obtained.

Based on the small signal model, the specific expressions of the voltage balancer are ((A4) shown at the top of the next page).

$Y_{\rm L1}$, $Y_{\rm L2}$, and $Y_{\rm L3}$ are the admittances of the load units: load unit 1, load unit 2, and load unit 3, respectively, and $Z_{\rm LC}$ is the impedance of the input filter

$$Z_{\rm LC} = \frac{sL}{(1 + LCs^2)}. \tag{A5}$$

The derivation of $Y_{\rm L1}$, $Y_{\rm L2}$, and $Y_{\rm L3}$ is to solve the input admittance of the small signal model.

Based on Fig. 27, the input impedance $Z_{\rm input}$ of the inner control loop can be obtained and the closed-loop input impedance

$$Z_1 = Z_2 \frac{sLR + s^2LCRR_{\rm C}}{2(1 + G_{\rm c}(s)F_{\rm m}(s)G_{\rm vd}(s)H(s))(sL + s^2LCR_{\rm C} + R + sCRR_{\rm C} + s^2LCR)}. \tag{A4}$$

$Z_{\rm cin}$ can also be deduced

$$Z_{\rm input} = \frac{\hat{v}_{\rm g}}{\hat{i}_{\rm in}} = \frac{1}{\frac{1}{Z_{\rm in}} - \frac{F_{\rm m}G_{\rm ind}[F_{\rm v}G_{\rm vg} + F_{\rm L}G_{\rm ig} + F_{\rm g}]}{1 + F_{\rm m}(F_{\rm v}G_{vd} + F_{\rm L}G_{\rm i}{\rm d})}} \tag{A6}$$

$$Z_{\rm cin} = \frac{1}{\frac{1}{Z_{\rm in}} - \frac{F_{\rm m}G_{\rm ind}[G_{\rm vg}(F_{\rm c}G_{\rm c}H_{\rm v} + F_{\rm v}H_{\rm vs}) + F_{\rm L}H_{\rm cs}G_{\rm ig} + F_{\rm g}]}{1 + F_{\rm m}[G_{\rm vd}(F_{\rm c}G_{\rm c}H_{\rm v} + F_{\rm v}H_{\rm vs}) + F_{\rm L}H_{\rm cs}G_{\rm id}]}}. \tag{A7}$$

As a result, $Y_{\rm i}$ can be represented as

$$Y_{\rm i} = \frac{1}{Z_{\rm in}} - \frac{F_{\rm m}G_{\rm ind}[G_{\rm vg}(F_{\rm c}G_{\rm c}H_{\rm v} + F_{\rm v}) + F_{\rm L}H_{\rm cs}G_{\rm ig} + F_{\rm g}]}{1 + F_{\rm m}[G_{\rm vd}(F_{\rm c}G_{\rm c}H_{\rm v} + F_{\rm v}) + F_{\rm L}G_{\rm id}]}. \tag{A8}$$

The specific expressions of the admittances are

$$\begin{aligned} Y_{\rm L1} = Y_{\rm L2} = Y_{\rm L3} = {} & \frac{D^2G_{\rm c}({\rm s})F_{\rm m}({\rm s})G_{vd}({\rm s})H_{\rm v}({\rm s})}{R(1+G_{\rm c}({\rm s})F_{\rm m}({\rm s})G_{vd}({\rm s})H_{\rm v}({\rm s}))} \\ & + \frac{sL(1+sCR_C+sCR)+R(1+sCR_C)}{D^2(1+G_{\rm c}({\rm s})F_{\rm m}({\rm s})G_{vd}({\rm s})H_{\rm v}({\rm s}))(1+sCR_C+sCR)}. \end{aligned} \tag{A9}$$

REFERENCES

[1] R. H. Lasseter and P. Paigi, "Microgrid: A conceptual solution," in *Proc. IEEE 35th Annu. Power Electron. Spec. Conf.*, 2004, vol. 6, pp. 4285–4290.

[2] J. M. Guerrero, J. C. Vasquez, J. Matas, L. G. de Vicuna, and M. Castilla, "Hierarchical control of droop-controlled AC and DC microgrids—A general approach toward standardization," *IEEE Trans. Ind. Electron.*, vol. 58, no. 1, pp. 158–172, Jan. 2011.

[3] T. Dragicevic, X. Lu, J. C. Vasquez, and J. M. Guerrero, "DC microgrids—Part I: A review of control strategies and stabilization techniques," *IEEE Trans. Power Electron.*, vol. 31, no. 7, pp. 4876–4891, Jul. 2016.

[4] M. Leng, S. Sahoo, F. Blaabjerg, and M. Molinas, "Projections of cyber-attacks on stability of dc microgrids—Modeling principles and solution," *IEEE Trans. Power Electron.*, vol. 37, no. 10, pp. 11774–11786, Oct. 2022.

[5] M. Leng, G. Zhou, H. Li, G. Xu, F. Blaabjerg, and T. Dragičević, "Impedance-based stability evaluation for multibus dc microgrid without constraints on subsystems," *IEEE Trans. Power Electron.*, vol. 37, no. 1, pp. 932–943, Jan. 2022.

[6] Y. Xia, W. Wei, M. Yu, X. Wang, and Y. Peng, "Power management for a hybrid AC/DC microgrid with multiple subgrids," *IEEE Trans. Power Electron.*, vol. 33, no. 4, pp. 3520–3533, Apr. 2018.

[7] P. Pan et al., "An impedance-based stability assessment methodology for DC distribution power system with multivoltage levels," *IEEE Trans. Power Electron.*, vol. 35, no. 4, pp. 4033–4047, Apr. 2020.

[8] Q. Tian, G. Zhou, L. Wang, Q. Bi, and M. Leng, "Symmetric bipolar output full-bridge four-port converter with phase-shift modulated buck–boost voltage balancer," *IEEE Trans. Ind. Electron.*, vol. 69, no. 8, pp. 8040–8054, Aug. 2022.

[9] H. Kakigano, Y. Miura, and T. Ise, "Low-voltage bipolar-type DC microgrid for super high quality distribution," *IEEE Trans. Power Electron.*, vol. 25, no. 12, pp. 3066–3075, Dec. 2010.

[10] F. Gao and D. Rogers, "Duty-cycle plus phase-shift control for a dual active half bridge based bipolar DC microgrid," in *Proc. IEEE App. Power Electron. Conf . Expo.*, 2018, pp. 1479–1485.

[11] Q. Tian, G. Zhou, H. Li, Y. Yang, and D. Zhou, "Symmetrical bipolar output isolated four-port converters based on center-tapped winding for bipolar DC bus applications," *IEEE Trans. Power Electron.*, vol. 37, no. 2, pp. 2338–2351, Feb. 2022.

[12] Y. J. Gu, W. H. Li, and X. N. He, "Analysis and control of bipolar LVDC grid with DC symmetrical component method," *IEEE Trans. Power Syst.*, vol. 31, no. 1, pp. 685–694, Jan. 2016.

[13] F. Wang, Z. Lei, X. Xu, and X. Shu, "Topology deduction and analysis of voltage balancers for DC microgrid," *IEEE Trans. Emerg. Sel. Topics Power Electron.*, vol. 5, no. 2, pp. 672–680, Jun. 2017.

[14] L. Tan, B. Wu, V. Yaramasu, S. Rivera, and X. Guo, "Effective voltage balance control for bipolar-DC-bus-fed EV charging station with three-level DC–DC fast charger," *IEEE Trans. Ind. Electron.*, vol. 63, no. 7, pp. 4031–4041, Jul. 2016.

[15] S. Rivera, R. Lizana, S. Kouro, T. Dragicevic, and B. Wu, "Bipolar DC power conversion: State-of-the-art and emerging technologies," *IEEE Trans. Emerg. Sel. Topics Power Electron.*, vol. 9, no. 2, pp. 1192–1204, Apr. 2021.

[16] B. He, W. Chen, X. Ruan, X. Zhang, Z. Zou, and W. Cao, "A generic small-signal stability criterion of DC distribution power system: Bus node impedance criterion (BNIC)," *IEEE Trans. Power Electron.*, vol. 37, no. 5, pp. 6116–6131, May 2022.

[17] M. Su, Z. Liu, Y. Sun, H. Han, and X. Hou, "Stability analysis and stabilization methods of DC microgrid with multiple parallel-connected DC–DC converters loaded by CPLs," *IEEE Trans. Smart Grid.*, vol. 9, no. 1, pp. 132–142, Jan. 2018.

[18] S. D. Tavakoli, P. Zhang, X. Lu, and M. Hamzeh, "Mutual interactions and stability analysis of bipolar DC microgrids," *CSEE J. Power Energy Syst.*, vol. 5, no. 4, pp. 444–453, Dec. 2019.

[19] R. D. Middlebrook, "Input filter considerations in design and application of switching regulators," in *Proc. IEEE Ind. Appl. Soc. Annu. Meeting*, 1976, pp. 366–382.

[20] X. Zhang, X. Ruan, and C. K. Tse, "Impedance-based local stability criterion for DC distributed power systems," *IEEE Trans. Circuits Syst. I, Reg. Papers*, vol. 62, no. 3, pp. 916–925, Mar. 2015.

[21] F. Liu, J. Liu, H. Zhang, and D. Xue, "Stability issues of $Z + Z$ type cascade system in hybrid energy storage system (HESS)," *IEEE Trans. Power Electron.*, vol. 29, no. 11, pp. 5846–5859, Nov. 2014.

[22] B. He, W. Chen, H. Mu, D. Zhan, and C. Zhang, "Small-signal stability analysis and criterion of triple-stage cascaded DC system," *IEEE Trans. Emerg. Sel. Topics Power Electron.*, vol. 10, no. 2, pp. 2576–2586, Apr. 2022.

[23] J. Sun, "Impedance-based stability criterion for grid-connected inverters," *IEEE Trans. Power Electron.*, vol. 26, no. 11, pp. 3075–3078, Nov. 2011.

[24] X. Feng, J. Liu, and F. C. Lee, "Impedance specifications for stable DC distributed power systems," *IEEE Trans. Power Electron.*, vol. 17, no. 2, pp. 157–162, Mar. 2002.

[25] P. Prabhakaran and V. Agarwal, "Novel four-port DC–DC converter for interfacing solar PV–fuel cell hybrid sources with low-voltage bipolar DC microgrids," *IEEE J. Emerg. Sel. Topics Power Electron.*, vol. 8, no. 2, pp. 1330–1340, Jun. 2020.

[26] M. Leng, G. Zhou, Q. Tian, G. Xu, and X. Zhang, "Improved small-signal model for switching converter with ripple-based control," *EEE Trans. Ind. Electron.*, vol. 68, no. 1, pp. 222–235, Jan. 2021.

Minrui Leng (Student Member, IEEE) received the B.S. degree in electrical engineering and automation from Southwest Jiaotong University, Chengdu, China, in 2014, and the Ph.D. degree from the School of Electrical Engineering, Southwest Jiaotong University, in 2021.

From 2019 to 2021, she was a visiting Ph.D. student with the Department of Energy Technology, Aalborg University, Aalborg, Denmark. She is currently an Assistant Professor with the College of Electrical Engineering, Sichuan University, Chengdu, China. Her research interests include small-signal modeling and dynamical modeling of power converters, control techniques of power converters, stability of distributed power systems and model predictive control, and cyberattacks of dc microgids.

Guohua Zhou (Senior Member, IEEE) received the B.S. degree in electronic and information engineering and the M.S. and Ph.D. degrees in electrical engineering from Southwest Jiaotong University, Chengdu, China, in 2005, 2008, and 2011, respectively.

From March 2010 to September 2010, he was a Research Assistant with the Department of Electronic and Information Engineering, Hong Kong Polytechnic University, Hong Kong. From October 2010 to March 2011, he was a Visiting Scholar (also a joint Ph.D. student) with the Center for Power Electronics Systems, Virginia Polytechnic Institute and State University, Blacksburg, VA, USA. He is currently a Professor with the School of Electrical Engineering, Southwest Jiaotong University. His research interests include modulation and control techniques of power electronics systems, dynamical modeling and analysis of switching power converters, and renewable energy applications of power electronics.

Guodong Xu was born in Henan, China, in 1996. He received the B.S. degree in electrical engineering and automation from Huaqiao University, Xiamen, China, in 2018, and the M.S. degree in electrical engineering from Southwest Jiaotong University, Chengdu, China, in 2021.

His research interests include modeling and stability analysis of cascaded systems.

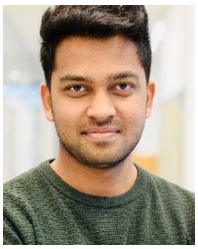

Subham Sahoo (Member, IEEE) received the B.Tech. degree in electrical and electronics engineering from Veer Surendra Sai University of Technology, Burla, India, in 2014, and the Ph.D. degree in electrical engineering from the Indian Institute of Technology, Delhi, New Delhi, India, in 2018.

He is currently an Assistant Professor with the Department of Energy, Aalborg University, Aalborg, Denmark, where he is also the Vice-Leader of the research group on the Reliability of Power Electronic Converters. His research interests include control, optimization, stability, and cybersecurity of power electronic systems.

Dr. Sahoo chairs the cybersecurity working group in the IEEE PELS Technical Committee (TC 10) on Design Methodologies. In 2020, he was a distinguished reviewer for IEEE TRANSACTIONS ON SMART GRID. He was a recipient of the Indian National Academy of Engineering Innovative Students Project Award for the best Ph.D. thesis across all the institutes in India in 2019.

Xueshan Liu (Member, IEEE) received the B.S. degree in communication engineering and the M.S. and Ph.D. degrees in electrical engineering from Southwest Jiaotong University, Chengdu, China, in 2005, 2010, and 2016, respectively.

From 2005 to 2008, he was a Development Engineer for switching mode power supplies in Asia Power Devices, Inc., Shenzhen, China. From 2010 to 2016, he was a Senior Application Engineer at O2micro International Limited, Chengdu, China. He is currently an Associate Professor with the College of Electrical Engineering, Sichuan University. His research interests include the control technique of switching mode power supply, power factor correction converters, and the application of power electronic systems.

Qun Zhou received the B.S. and Ph.D. degrees in automation engineering from the University of Electronic Science and Technology of China, Chengdu, China, in 1989 and 2009, respectively.

Since 1989, she has been with the School of Electrical Engineering Information, Sichuan University, Chengdu, China, where she has been an Associate Professor, since 1998. Her research interests include power quality analysis and control.

Yue Yin (Member, IEEE) received the B.S. degree in School of mechanical and energy engineering from Jimei University, Xiamen, China, in 2006, the M.S. degree in control science and engineering from Sichuan University, Chengdu, China, in 2010 and the Ph.D. degree in electrical engineering from Sichuan University, Chengdu, China, in 2020.

She was a visiting Ph.D. student at Stevens Institute of Technology, Hoboken, NJ, the USA from 2019 to 2020. She is currently an Associate Professor with the College of Electrical Engineering, Sichuan University, Chengdu, China. Her research interests include stochastic optimization on power system operation and planning with renewable energy.

Frede Blaabjerg (Fellow, IEEE) received the Ph.D. degree in electrical engineering from Aalborg University, Aalborg, Denmark, in 1995.

From 1987 to 1988, he was with ABB-Scandia, Randers, Denmark. He became an Assistant Professor in 1992, an Associate Professor in 1996, and a Full Professor of power electronics and drives in 1998. In 2017, he became a Villum Investigator. He is *honoris causa* at University Politehnica Timisoara, Romania, and Tallinn Technical University, Tallinn, Estonia. He has authored or coauthored more than 600 journal papers in the fields of power electronics and its applications. He is the coauthor of four monographs and an editor of ten books on power electronics and its applications. His research interests include power electronics and its applications, such as in wind turbines, PV systems, reliability, harmonics, and adjustable speed drives.

Dr. Blaabjerg was the Editor-in-Chief of the IEEE TRANSACTIONS ON POWER ELECTRONICS from 2006 to 2012. He was a Distinguished Lecturer for the IEEE Power Electronics Society from 2005 to 2007 and for the IEEE Industry Applications Society from 2010 to 2011 and 2017 to 2018. During 2019–2020 he was the President of IEEE Power Electronics Society. He is currently the Vice-President of the Danish Academy of Technical Sciences too. He was the recipient of 32 IEEE Prize Paper Awards, the IEEE PELS Distinguished Service Award in 2009, the EPE-PEMC Council Award in 2010, the IEEE William E. Newell Power Electronics Award in 2014, the Villum Kann Rasmussen Research Award in 2014, the Global Energy Prize in 2019, and the 2020 IEEE Edison Medal. He was nominated in 2014–2019 by Thomson Reuters to be among the most 250 cited researchers in Engineering in the world.